

Single-Molecule Electronic Measurements with Metal Electrodes

Stuart Lindsay

Department of Physics and Astronomy, and Department of Chemistry and Biochemistry, and the Biodesign Institute, Arizona State University, Tempe, AZ 85287; Stuart.Lindsay@asu.edu

I begin this article with a section that reviews the underlying concepts. This is followed by a discussion of experimental approaches for single-molecule measurements. Finally some of the problems and challenges are listed. The topics primarily use examples from our lab, though I have attempted to set these in the context of other work.

Concepts

Tunneling through a Metal–Molecule–Metal Junction

The first problem to tackle is that of a molecule weakly connected to electrodes. In this context, “weak” means that the quantum “resistance” associated with the barrier between the metal and the molecule is much greater than the Landauer resistance (see the contribution by Tao in this issue). That is, if the only constriction in the system were the “contact” component, then $T \ll 1$ for this component constitutes weak coupling.

The conventional one-dimensional picture of electron tunneling is that of a potential step barrier of height V_0 and width L . In this picture, an incident electron of energy $E (= \hbar^2 k^2 / 2m)$ and wavefunction e^{ikx} impinges on the barrier, with its wavefunction in the barrier region changing to $e^{-\kappa x}$ with $(\hbar^2 \kappa^2 / 2m) = V_0 - E$ (1). The transmission probability through the barrier is approximately proportional to $e^{-\beta L}$, with the decay parameter β being 2κ . Thus for monoenergetic electrons, the current passing through the barrier is expected to decrease as the barrier thickness increases, and the rate of decrease (β) depends on the electron energy

$$\beta = 2\sqrt{\frac{2m\varphi_0}{\hbar^2}} = 1.02 \sqrt{\frac{\varphi_0}{eV}} \text{ \AA} \quad (1)$$

where φ_0 is the barrier height $V_0 - E$.

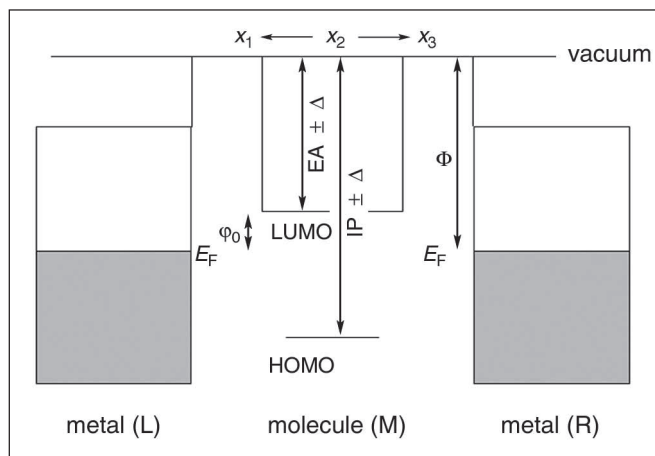
Figure 1. Schematic plot of energy (vertical distance) versus distance (horizontal axis) for a metal–molecule–metal junction. For the transport properties to be dominated by the molecule, the physical gap between the electrodes and the molecule (x_1, x_3) must be much less than the width of the molecule (x_2). However, these gaps must be big enough so that the interaction between the molecular states and the metals is small. Here, the lowest-unoccupied molecular orbital (LUMO) and highest-occupied molecular orbital (HOMO) are related to the electron affinity (EA) and ionization potential (IP) as corrected for the energy difference between charged and uncharged states (Δ). Current is carried by electrons at the Fermi energy (E_F) located below the vacuum by a quantity of energy equal to the work function, Φ .

How does this conventional picture carry over to tunneling through a molecule, and how is β expected to depend on the applied voltage? A significant change is that the barrier is replaced by a set of molecular orbitals on the molecule. Considering a very long chain, the molecular orbitals become bands in which the energy has a momentum dependence parameterized by an effective mass m^* . For the finite length molecule, a first approximation for the orbitals is that they are the band states of the infinite chain but with wavelengths commensurate with the short chain. The result of this analysis is that the barrier picture is modified to one where m is replaced by m^* and the barrier height is the energy difference of the electron in the contact and that of the molecular orbital (2).

So, for a metal–contact system, a first approximation is that the barrier height becomes $\varphi_0 = (E_{\text{LUMO}} - E)$ for tunneling through the molecular LUMO, or $\varphi_0 = (E - E_{\text{HOMO}})$ for tunneling through the molecular HOMO, and the decay constant β is

$$\beta = 2\sqrt{\frac{2m^*(E_{\text{LUMO}} - E)}{\hbar^2}} \quad (2)$$

E in eq 2 is the energy of the incident electron, equal, at zero bias, to the Fermi energy of the metal contact (Figure 1). However, the application of a bias to the junction (to drive a net current) alters this energy (see below). As the length of the molecule in the gap is varied, so is the tunneling probability. The tunneling probability is also varied by changing the voltage. These changes give us signatures of the tunneling process and an indication of how far the molecule is from resonance (where $E = E_{\text{LUMO}}$ or $E = E_{\text{HOMO}}$). A qualitative picture is shown in Figure 1. Starting with left (L) and right



(R) metallic contacts in equilibrium with the molecule (M) connecting them, the Fermi levels E_F of the contacts line up and the barrier height φ_0 is the energy difference between the LUMO level of the molecule and the Fermi level of the contacts. This barrier is, in general, much less than the intrinsic barrier, the work function Φ , so the molecule serves to enhance tunneling over the vacuum case. For this picture to apply, the region between the metal and the molecule must be physically thin compared to the length of molecule (yet thick enough so that the weak-coupling approximation holds). A voltage, V , applied to the right contact lowers its electron energy levels by V relative to the left contact. We assume that the molecular-orbital charge density is uniformly distributed over the molecule; this results in the first-order perturbation-theory estimate of the energy shift of the LUMO to be $V/2$ relative to the contacts, since first-order perturbation theory shifts energy levels according to the average perturbation over that orbital's charge density. This approximation treats the contacts L and R symmetrically. In this simple picture, we can write β as

$$\beta = 2\sqrt{\frac{2m^*\left(\varphi_0 - \frac{V}{2}\right)}{\hbar^2}} \quad (3)$$

When the molecular orbital lines up with the Fermi level, $\varphi_0 = V/2$, resonant tunneling occurs and $\beta = 0$. For some geometries, the transmission of the gap goes to unity, so that the resistance would become equal to the Landauer resistance (3).

In practice, voltages big enough to drive a resonance are only usually applied in a clean vacuum where clear signs of resonant tunneling have been observed (4). Outside of ultrahigh vacuum, environmental polarization will cause "resonance" to occur at a lower energy. In the event that the polarization is well defined (i.e., in a standard salt solution) then the process is best described as a local redox reaction.

Contrast with Electrochemical and Optical-Charge Injection

Data for charge-transport rates measured optically (i.e., via an attached fluorophore that is optically excited; ref 5) or electrochemically (6) share some common physics with the problem discussed here (7). However, the connection is neither simple nor direct. Electrons are injected by states with a different energy (and density distribution) from those injected by metal electrodes, and similarly, can be accepted by states with a different energy (and density distribution) from those entering metal electrodes. Thus comparison of electron-transfer rates between the various techniques can be complicated, though certain gross features remain unchanged. For example, electron transfer via a long alkane chain will be slow no matter the source and sink of electrons, as long as resonance is avoided.

The Strong-Coupling Limit

Paradoxically, much of the electronic signal characteristic of a molecule is lost when the bonding to metal contacts is strong because of the mixing of states that occurs. Thus, a single H_2 molecule bridging two Pt electrodes transmits at

essentially unity quantum efficiency (8). Localized electronic states can, apparently, be detected in this limit, but via indirect many-body effects (e.g., the Kondo effect; ref 9).

Detailed Calculations of Tunnel Transport

Calculations of the theoretical current–voltage curves are usually based on the Landauer–Buttiker formalism (10, 11) with the transmission function calculated using quantum-mechanical scattering theory (12, 13). The current is calculated as

$$I(V) = \frac{2e^2}{h} \int T(E, V) \left[f\left(E - \frac{eV}{2}\right) - f\left(E + \frac{eV}{2}\right) \right] dE \quad (4)$$

where $T(E, V)$ is the transmission function (12, 13), f is the Fermi function, and V is the voltage. The transmission function is

$$T(E, V) = \text{tr} \left[\Gamma_L \left(E - \frac{eV}{2} \right) G_M(E) \Gamma_R \left(E + \frac{eV}{2} \right) G_M^*(E) \right]$$

where G_M represents the Green's function matrix elements for the coupled system (metal–molecule–metal). These elements can be worked out using standard quantum-chemical methods, or more simply (and more approximately), for large systems, density-functional methods based on the local density approximation (as describe in other contributions). However, it is important to note that these matrix elements are *exponentially sensitive to the geometry of bonding in the system*. Therefore, the connection between "components" of the system can vary all the way from $T = 1$ for well-connected, isoenergetic components, to $T = 0$ for components aligned so that there is no wavefunction overlap. *Thus, atomistic control of the structure is required for reliable data.*

Electron Transfer through Redox-Active Molecules

If the molecule in the gap has a well-defined acceptor state (or donor state, with appropriate modification of what is discussed below), then redox processes may contribute to the observed current. The steps are shown schematically in Figure 2. The energy level marked "LUMO" corresponds to the location of the LUMO in the unoccupied molecule (i.e., the state that would mediate virtual tunneling transitions in the discussion above). The parabola that sits on top of this state represents fluctuations away from the local minimum caused by the coupling of electronic energy to environmental fluctuations (Marcus showed that such potential surfaces are often well described by parabolas). The state labeled "REDOX" corresponds to the energy of an occupied LUMO, as lowered by the environmental-polarization response to the charging (the circle with a "+" in it represents an ion that has moved in to maintain charge neutrality of the now-charged LUMO, thereby lowering its electrostatic energy). This REDOX level is also coupled to environmental fluctuations, resulting in the parabolic fluctuation of its energy with time as shown by the parabola imposed on top of this level. In step A of the charge-transfer process, fluctuations eventually take the LUMO parabola up to an energy where it intersects the REDOX parabola (dark curved arrow). At that point, total electronic energy is lowered by occupation of the REDOX level and the electron relaxes down to this

level, now trapped on the molecule. In the second phase of the charge transfer (Figure 2B), the trapped electron is released as a fluctuation takes the energy of the occupied REDOX state back into degeneracy with the energy of the unoccupied LUMO state (the positive ion having moved away from the molecule in this illustration). Now the electron can lower its energy still further by passing on to the Fermi level in the right electrode (which is lowered through the application of a bias voltage across the electrodes).

Because this process involves a sequential reduction and oxidation, the overall rate should maximize when the molecule is near its formal potential with respect to the electrode (assuming a small bias is applied) (14). This effect was demonstrated using the STM contrast of images of iron-containing porphyrin molecules on a graphite electrode in the classic article by Tao (15).

Useful though these ideas are (see the review by Mazur and Hipps; ref 16), the exact nature of polarization on an electrode surface, even in supporting electrolyte, is problematical when a second electrode is nearby. This issue is yet more difficult when measurements are made in the solid state with no attempt to control the surface potential of electrodes. Nonetheless, the expectation is that tunneling rates will be enhanced by transitions that involve redox processes and that the energy at which these states become accessed will be less than that of the LUMO (vice versa for the HOMO and hole

transport) as involved in vacuum-resonant tunneling. Single-molecule measurements are further complicated by the noise associated with few-atom processes, a point to which we will return.

Single-Molecule Measurements

Almost all of the measurements made to date that claim to be single-molecule have been made using gold electrodes, most often in a break-junction geometry (17). Gold is malleable and ductile and, when covered with a layer of thiolated molecules, almost liquid-like at its surface (see below). We will review break junctions, the self-assembled junctions developed in my lab and the nanoscale assembly of fixed gaps. It should be noted that the literature is replete with "single-molecule" data that, for a given molecule, span orders of magnitude in the value of current measured at a given bias (18) so the subject needs to be approached with caution.

Break Junctions

Break junctions are formed by cracking a gold filament with controlled strain of a substrate. By covering the gold with molecules bis-functionalized with thiols, the hope is that one, or a few molecules will span the gap as it is cracked open. The first such data were demonstrated for benzenedithiol by Reed and coworkers (17). With better manufacturing of the gold filament, and the use of clean conditions, reliability has been improved (19). Techniques have also been developed to adsorb a molecule in the gap and trap it at low temperatures (20). The resulting current-voltage characteristics, obtained in a cryo vacuum, show distinct steps at the same voltages in both forward and reverse bias, consistent with a resonant-tunneling process.

The measurements discussed above suffer from a paucity of data. There are clearly significant molecule-to-molecule variations, so there is a need to characterize a large number of molecules. Xu and Tao (21) have an elegant solution to this problem. They operate an STM as an automated break junction, pushing a gold tip (under computer control) into a gold substrate immersed in a solution of dithiolated molecules. The bias between tip and substrate is fixed and the current recorded as the tip is pulled away from the surface. The current versus distance plots show discrete plateaus (regions of constant current over a significant distance of the pull) corresponding to integral numbers of molecules bridging the gap (this is known because of the single-molecule "calibration" data determined from the somewhat more complex method of self-assembled junctions described below). When these values of current plateau are histogrammed, distinct peaks are seen in the conductance, corresponding to 1, 2, 3, ... molecules bridging the gap (21). The plateaus in the current versus distance plots form because gold filaments are very ductile, so a single molecule dominates the gap resistance as the gold to which it is attached is drawn out from the tip and substrate (22). This method is simple to carry out and gives reproducible data. However, it does not permit temperature to be varied significantly, and I-V curves must usually be assembled piecewise from a series of experiments run at different biases.

These experiments exploit the extreme mobility of gold surfaces. We have shown elsewhere that contacts to these sur-

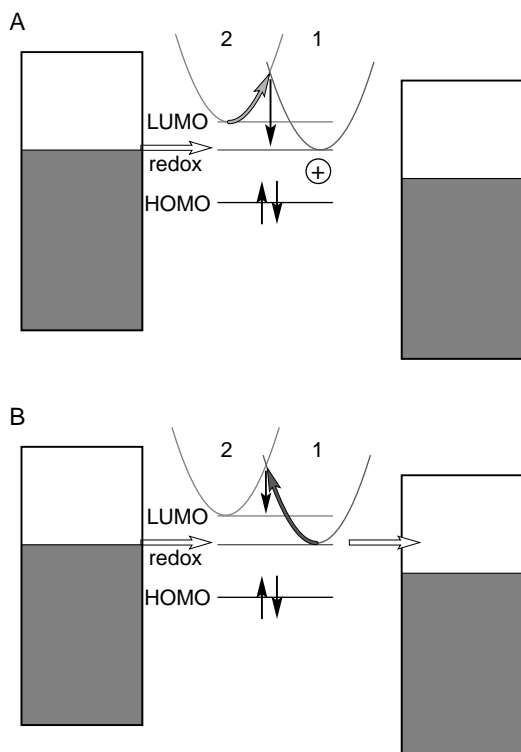


Figure 2. Schematic showing the steps in electron transfer involving a localized state (REDOX). The overall charge transfer requires a first reduction step (A) followed by a second oxidation step (B). The 1-D parabolas represent the paths along the potential surfaces that intersect at the lowest transition-state energy. See the text for details.

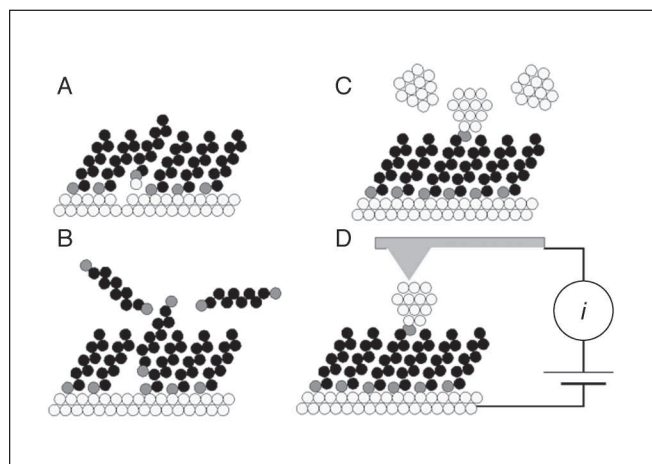


Figure 3. Self-assembly of a single-molecule metal–molecule–metal junction. Alkanethiols are removed from a monolayer (A) leaving holes for the insertion of dithiolated molecules (B), which are then contacted with gold nanoparticles (C). The resulting metal–molecule–metal junction is contacted on the top side with a conducting atomic force microscope (D).

Figure 4. (A) Typical I–V curves obtained from a self-assembled junction as illustrated in Figure 3. The curves have the property that the current at each voltage is an integer multiple of some fundamental current (B).

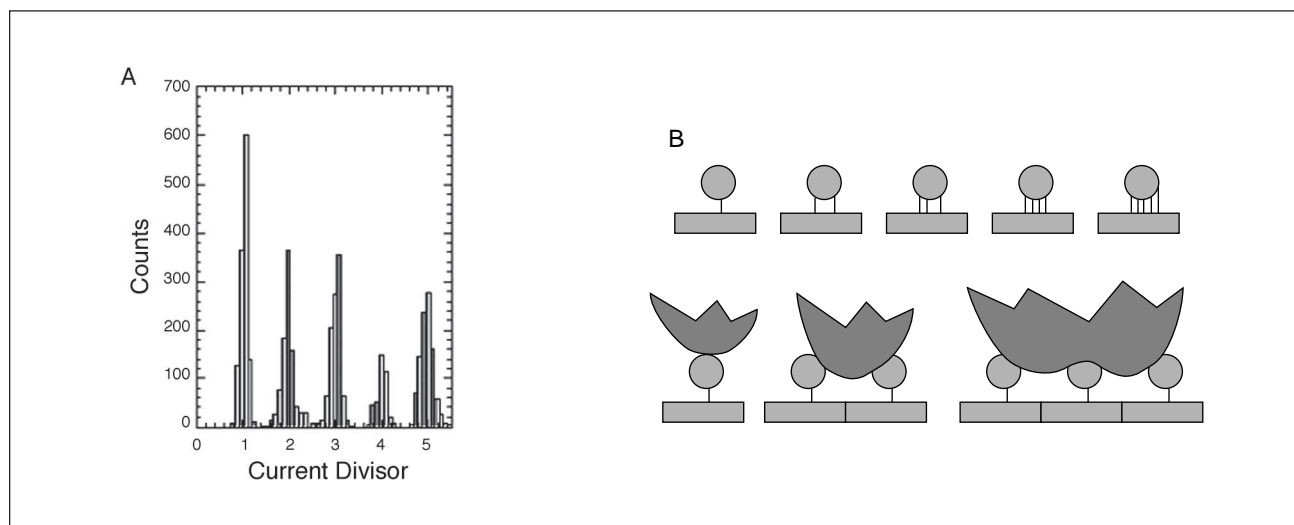
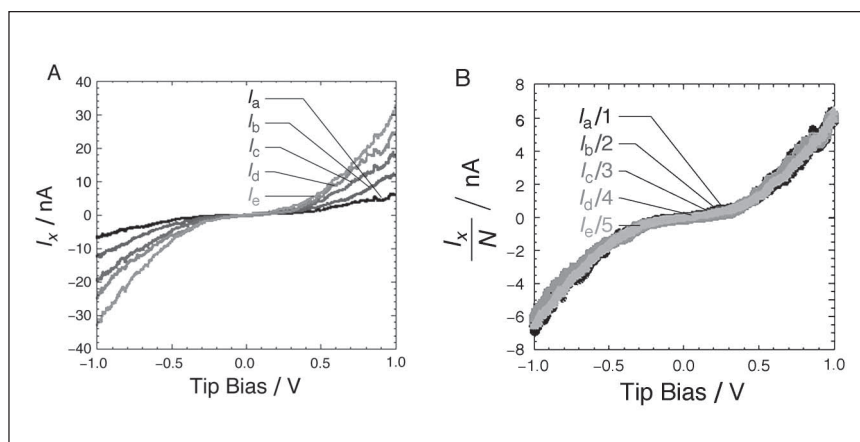


Figure 5. Curves like those shown in Figure 4 are related by integer multiples of a fundamental curve as shown by a computer analysis of many curves (A). There are over 1000 curves in the single-molecule bin ($X = 1$). Possible models for the observed quantization of the I–V curves are (B top) multiple molecules connecting the nanoparticle to the substrate or (B bottom) the AFM probe contacting several nanoparticles at once.

faces undergo significant fluctuations at room temperature, resulting in the apparent spontaneous on–off switching in molecular conduction (23). Thus, the very malleability on which these techniques rely is also a source of potential unreliability should gold contacts be used in device applications.

Self-Assembled Nanojunctions

We have developed a method to self-assemble single-molecule devices with the molecules set in a well-defined geometry with covalent bonds to two gold contacts (24). The process is shown schematically in Figure 3. A self-assembled monolayer of (in this case) octanethiol is placed in contact with a solvent (Figure 3A) so that some molecules leave (taking a gold atom with them, such is the lability of the gold surface covered with thiols; ref 25). Thus, such a surface, when placed in a solution of dithiolated molecules, will open up spaces for the dithiolated molecules to enter the monolayer, as shown in Figure 3B (26). The result is dithiolated molecules inserted into a monolayer of monothiols in a well-defined orientation and bonded at their lower end to the gold substrate. It is still not easy to make an electrical contact to the inserted molecules, because the atoms of a top contact must line up correctly with the (now fixed) upper thiol, so that a chemical bond can form. To solve this problem, the monolayer is next incubated with a suspension of gold nanoparticles (NPs) (Figure 3C). We used 1.5-nm diameter gold stabilized with triphenylphosphine as this ligand is readily displaced by the more reactive thiol. The NPs find the protruding thiols and attach to them. The attached NPs then make excellent “large” targets for a conducting atomic force microscope (AFM) probe. A gold-coated probe is pushed into the NP to complete a circuit as shown schematically in Figure 3D.

A set of I–V curves measured for octanedithiol are shown in Figure 4A. They have the remarkable property that, when divided by the appropriate integer, they all collapse to a universal curve as shown in Figure 4B. This property is quite general. The comparison of curves can be automated with a program that finds a divisor such that the variance of one curve with respect to another is minimized. When chosen so that the ratios are one or greater, the distribution of this divisor shows sharp peaks at integer values, confirming the quantized nature of the current–voltage curves (Figure 5A). Two models for this behavior are shown in Figure 5B. The upper model shows one gold “ball” connecting one, two, three, et cetera, molecules from the ball to the substrate. The lower model shows a blunt AFM tip contacting multiple balls on the surface. In either case, the molecules act like resistors wired in parallel to give curves in which the currents are integer multiples of each other. The monothiol molecules in the matrix make no significant contribution to the current and can be ignored.

The single-molecule I–V curve is quite close to what is calculated from a first-principles theory with no adjustable parameters (24), and this is an enormous improvement on earlier comparisons of theory and experiment (18). However, the residual disagreement is quite interesting. Figure 6 shows a single-molecule I–V curve on which straight lines have been imposed. Typical tunneling characteristics are linear at low bias (consistent with line a) but should take off exponentially at higher bias, quite inconsistent with the subsequent linear

regions labeled b in the figure. In fact, in this range of bias, the calculated I–V curve is essentially Ohmic (i.e., linear) with a gradient close to the lines labeled b. Thus, it appears that the molecule is “switched off” at low bias. Such switching behavior is a characteristic of Coulomb blockading (27), a process in which current is inhibited until electrons have the energy required to charge the NP. The only requirement for the NP to charge independently of the probe is that the contact resistance between the AFM probe and the NP exceeds the Landauer resistance. This is quite likely, as a lack of strong adhesion between the AFM probe and NP indicates that good metallic bonds are not being made.

The current–voltage curves of several different lengths of alkane chains yield an anomalous value for β when analyzed without taking account of the Coulomb blockade (28). Using the Hanna–Tinkham model for Coulomb blockading (27), Tomfohr fitted these data (29) finding a consistent value for the intrinsic capacitance associated with the sphere (and also a value close to that yielded by simple estimates based on the NP geometry). The resistances associated with the molecule (as extracted from these fits) agreed well with the resistances calculated from first principles and were consistent with a much more reasonable value for β (of 1 per methylene), resolving the problems posed by the raw data (28). We have shown (unpublished data) that the region of suppressed current (i.e., between ± 0.5 V in Figure 6) gets larger when smaller spheres are used, consistent with the Coulomb blockade explanation. Perhaps most convincing, the parameters proved transferable to measurements made on carotenoids where excellent agreement was obtained between experiment and first-principles calculations modified to include the Coulomb blockade (30).

It is worth stressing that, for several molecules (various lengths of alkanes, a carotenoid) good agreement now exists between theory (with no adjustable parameters) and experiment. Thus, the large uncertainties that have plagued this field (18) have been dealt with in a few cases. There are loose ends. The resistance in the blocked region (line a in Figure 6) is considerably smaller than predicted from theory (where the current arises from thermal activation of electrons

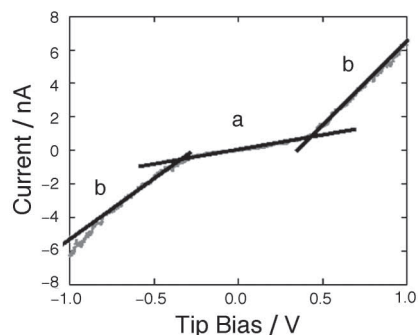


Figure 6. Showing how a single-molecule I–V curve for octanedithiol is Ohmic at low voltage (a) and then again at higher voltage (b) as opposed to the expected exponential behavior at higher bias. The explanation lies in a Coulomb blockade associated with the nanoparticle (see text).

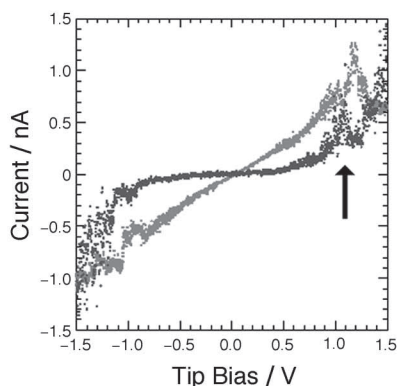


Figure 7. Current–voltage characteristics for 1-nitro-2,5-di(phenylethynyl-4'-thioacetyl)benzene. A negative differential resistance peak is pointed to by the arrow.

over the blockade barrier). Importantly, there is a need for variable temperature measurements on single molecules. Very little temperature dependence is expected for the tunneling mechanism, but this point should be checked for a single molecule (though self-assembled monolayers have been examined; ref 31).

Fixed Nanogaps

Small gaps, with the potential for being bridged by single molecules, have been made using electromigration (32) (essentially blowing a small “fuse” at a constriction) and using electrochemical methods both to etch and to fill-in small gaps (33). Some spectacular results have been reported using these approaches (9, 34). They do, however, require the selection of “good” devices and perhaps a little faith in the nature of the nanostructures that are formed. For example, interesting and complex characteristics are found in electromigration gaps *not* exposed to molecules (35). These structures have certainly proved difficult to work with in our laboratory.

In a remarkable tour-de-force, Kubatkin et al. (36) have exploited the complexity of these nanogaps to make simple junctions. Their work is based on a low-temperature study of junctions made by careful evaporation of Au into a nanojunction structure on a clean surface at low temperature. Metal islands were allowed to form in a controlled way, and the resulting metal–metal island–metal structures characterized using the consequent single-electron transistor characteristics (37). One side of the island was then connected to a bulk electrode by further evaporation, leaving behind a gap that had been precisely calibrated with single-electron transistor measurements. Oligophenylene–vinylene molecules were sublimed into the gap and the device warmed until a single molecule became trapped in the gap. The application of a gate voltage revealed a series of Coulomb blockade states associated with multiple electronic occupation of states of the molecule. The energies of the states were in agreement with a many electron (Hubbard model) Hartree–Fock calculation. This is a remarkable achievement, but the technique is far from routine, and only a few molecules were measured for the original report (36).

Problems and Challenges

Electrochemical Control and Redox-Mediated Processes

The beautiful experiment of Tao (15) probably succeeded as it did because the redox-active molecules on the graphite surface were probed with an STM. Thus, the perturbation of the molecules (and their environment) by the second electrode was presumably not dominant (as evidenced by the quantitative correlation between the thin-film voltammetry and the measured STM transmission). Can redox processes be observed with direct metal connections to a molecule?

We investigated 1-nitro-2,5-di(phenylethynyl-4'-thioacetyl)benzene molecules using the self-assembled nanogap techniques described above (38), motivated by the observation of negative differential resistance (NDR) in monolayers of these molecules (39). Current–voltage characteristics spanning the extremes of our data are shown in Figure 7. The arrow points to a peak in the current near the previously reported peak current in the bulk device. The NDR is clearly an intrinsic property of single molecules. Furthermore, molecules lacking the electroactive nitro group do not show this peak (38). Therefore, it is tempting to assume that the peak is associated with an electrochemical process. However, the opening of a redox channel should add current to the tunneling background, resulting in a step increase in the current as observed by Snyder and White (40). (Note that the peak in STM contrast reported in the Tao experiment is a consequence of the differential nature of the measurement: the current *in a small voltage window* was measured as a function of surface potential; ref 15.) Thus, the peak observed in the 1-nitro-2,5-di(phenylethynyl-4'-thioacetyl)benzene molecules (38) and films (39) is hard to understand. It may reflect the ill-defined electrochemical environment in these experiments. For example, a reaction involving a species dissolved in the monolayers would be limited by diffusion in the monolayers, resulting in a fall-off in current when the local concentration was depleted. The single molecule conductance of a redox-active molecule has recently been measured under potential control in an electrolyte (41).

Noise in Few-Atom Redox Processes

The I–V characteristics in Figure 7 are clearly noisy, reminiscent of the switching noise observed in a nanoscale conducting polymer wire as it was oxidized or reduced (42). This noise may be purely statistical and based on the small number of counter ions (or reactive species) involved in the switching process. This problem will have to be addressed if single-molecule devices are to be based on redox processes.

Atomistic Control of Connections

Kubatkin et al. (36) made random structures, selecting the desired ones with very sophisticated measurements. A great advance would come from controlled assembly of nanometer-scaled gaps in conductors. For example, self-assembled silicide nanowires might be coaxed into forming well-defined nanogaps (43). Even so, molecules designed for insertion into such gaps would have to accommodate relaxation of the atomic structure of the electrodes caused by the chemical bonding of the molecule to the electrodes.

Temperature Dependence

Measurement of changes in electrical properties with temperature lie at the core of our understanding of transport in solid-state devices. It is hard to see how single-molecule electronic devices can be constructed so as to remain mechanically stable over a large range of temperatures, but this needs to be done.

The above problems notwithstanding, significant progress has been made in understanding the electronic properties of molecules wired into electronic circuits. Whether or not a future generation of computer chips exploits these advances, the fundamental nature of charge transport in these systems is being revealed.

Acknowledgments

This work was supported by a NIRT award of the NSF, and represents many contributions from colleagues and students, among them Otto Sankey, Devens Gust, Tom Moore, Ana Moore, Nongjian Tao, Larry Nagahara, Alex Primak, Yuichi Terazano, Ganesh Ramachandran, Xiadong Cui, John Tomfohr, Fan Chen, and Jin He.

Literature Cited

- Liboff, R. L. *Introductory Quantum Mechanics*; Holden-Day Inc.: Oakland, CA, 1980.
- Tomfohr, J.; Sankey, O. F. *Phys. Stat. Sol. B-Basic Research* **2002**, *233*, 59–69.
- Kalmeyer, V.; Laughlin, R. B. *Phys. Rev.* **1987**, *B35*, 9805–9808.
- Guisinger, N. P.; Greene, M. E.; Basu, R.; Baluch, A. S.; Hersam, M. C. *Nano Letters* **2004**, *4*, 55–59.
- Williams, T. T.; Barton, J. K. Charge transport in DNA. In *DNA and RNA Binders: From Small Molecules to Drugs*; Demeunynck, M., Bailly, C., Eds.; Wiley-VCH: Weinheim, 2003; pp 146–172.
- Chidsey, C. E. D. *Science* **1991**, *251*, 919–922.
- Adams, D. M.; Brus, L.; Chidsey, C. E. D.; Creager, S.; Creutz, C.; Kagan, C. R.; Kamat, P. V.; Lieberman, M.; Lindsay, S.; Marcus, R. A.; Metzger, R. M.; Michel-Beyerle, M. E.; Miller, J. R.; Newton, M. D.; Rolison, D. R.; Sankey, O.; Schanze, K. S.; Yardley, J.; Zhu, X. *J. Phys. Chem.* **2003**, *107*, 6668–6697.
- Smit, R. H. M.; Noat, Y.; Untiedt, C.; Lang, N. D.; van Hemert, M. C.; Van Ruitenbeek, J. M. *Nature* **2002**, *419*, 906–909.
- Park, J.; Pasupathy, A. N.; Goldsmith, J. I.; Chang, C.; Yalsh, Y.; Petta, J. R.; Rinkoski, M.; Sethna, J. P.; Abruna, H. D.; McEuen, P. L.; Ralph, D. C. *Nature* **2002**, *417*, 722–725.
- Landauer, R. *J. Phys. Condens. Matter* **1989**, *1*, 8099–8110.
- Büttiker, Imry, Y.; Landauer, R.; Pinhas, S. *Phys. Rev.* **1985**, *B31*, 6207–6215.
- Mujica, V.; Kemp, M.; Ratner, M. A. *J. Chem. Phys.* **1994**, *101*, 6849–6855.
- Datta, S. *Electronic Transport in Mesoscopic Systems*; Cambridge University Press: Cambridge, 1990.
- Schmickler, W.; Tao, N. J. *Electrochim. Acta* **1997**, *42*, 2809–2815.
- Tao, N. *Phys. Rev. Letts.* **1996**, *76*, 4066–4069.
- Mazur, U.; Hipps, K. W. *J. Phys. Chem.* **1995**, *99*, 6684–6688.
- Reed, M. A.; Zhou, C.; Muller, C. J.; Burgin, T. P.; Tour, J. M. *Science* **1997**, *278*, 252–254.
- Salomon, A.; Cahen, D.; Lindsay, S.; Tomfohr, J.; Engelkes, V. B.; Frisbie, C. D. *Adv. Mater.* **2003**, *15*, 1881–1890.
- Reichert, J.; Ochs, R.; Beckmann, D.; Weber, H. B.; Mayor, M.; von Lohneysen, H. *Phys. Rev. Lett.* **2002**, *88*, 176804.
- Reichert, J.; Weber, H. B.; Mayor, M.; von Lohneysen, H. *Appl. Phys. Lett.* **2003**, *82*, 4137–4139.
- Xu, B.; Tao, N. *J. Science* **2003**, *301*, 1221–1223.
- Xu, B.; Xiao, X.; Tao, N. *J. Am. Chem. Soc.* **2003**, *125*, 16164–16165.
- Ramachandran, G. K.; Hopson, T. J.; Rawlett, A. M.; Nagahara, L. A.; Primak, A.; Lindsay, S. M. *Science* **2003**, *300*, 1413–1415.
- Cui, X. D.; Primak, A.; Zarate, X.; Tomfohr, J.; Sankey, O. F.; Moore, A. L.; Moore, T. A.; Gust, D.; Harris, G.; Lindsay, S. M. *Science* **2001**, *294*, 571–574.
- Sondag-Huethorst, J. A. M.; Schonenberger, C.; Fokkink, L. G. J. *J. Phys. Chem.* **1994**, *98*, 6826–6834.
- Cygan, M. T.; Dunbar, T. D.; Arnold, J. J.; Bumm, L. A.; Shedlock, N. F.; Burgin, T. P.; Jones, L.; Allara, D. L.; Tour, J. M.; Weiss, P. S. *J. Am. Chem. Soc.* **1998**, *120*, 2721–2732.
- Hanna, A. E.; Tinkham, M. *Phys. Rev. B* **1991**, *44*, 5919–5922.
- Cui, X. D.; Primak, A.; Zarate, X.; Tomfohr, J.; Sankey, O. F.; Moore, A. L.; Moore, T. A.; Gust, D.; Nagahara, L. A.; Lindsay, S. M. *J. Phys. Chem. B* **2002**, *106*, 8609–8614.
- Tomfohr, J. Electron Tunneling Transport Theory for Molecules. Ph.D. Thesis, Arizona State University, 2002.
- Ramachandran, G. K.; Tomfohr, J. K.; Sankey, O. F.; Li, J.; Zarate, X.; Primak, A.; Terazano, Y.; Moore, T. A.; Moore, A. L.; Gust, D.; Nagahara, L. A.; Lindsay, S. M. *J. Chem. Phys. B* **2003**, *107*, 6162–6169.
- Wang, W.; Lee, T.; Reed, M. A. *Phys. Rev. B* **2003**, *68*, 035416.
- Park, H.; Lim, A. K. L.; Alivisatos, A. P.; Park, J.; McEuen, P. L. *Appl. Phys. Lett.* **1999**, *74*, 301–303.
- Li, C. Z.; He, X. E.; Tao, N. *J. Appl. Phys. Lett.* **2000**, *77*, 3995–3997.
- Liang, W.; Shores, M. P.; Bockrath, M.; Long, J. R.; Park, H. *Nature* **2002**, *417*, 725–728.
- Lee, T.-H.; Dickson, R. M. *J. Phys. Chem. B* **2003**, *107*, 7387–7390.
- Kubatkin, S.; Danilov, A.; Hjort, M.; Cornil, J.; Bredas, J.-L.; Stuhr-Hansen, N.; Hedegard, P.; Bjornholm, T. *Nature* **2003**, *425*, 698–701.
- Kubatkin, S.; Danilov, A.; Olin, H.; Claesson, T. *J. Low Temp. Phys.* **2000**, *118*, 307–316.
- Rawlett, A.; Hopson, T. J.; Nagahara, L.; Tsui, R.; Ramachandran, G.; Lindsay, S. *Appl. Phys. Lett.* **2002**, *81*, 3043–3045.
- Chen, J.; Reed, M. A.; Rawlett, M. A.; Tour, J. M. *Science* **1999**, *286*, 1550–1552.
- Snyder, S. R.; White, H. S. *J. Electronanal. Chem.* **1995**, *394*, 177–185.
- Chen, F.; He, J.; Nuckolls, C.; Roberts, T.; Klare, J. E.; Lindsay, S. M. *Nano Lett.* published online Feb 18, 2005.
- He, H. X.; Li, X. L.; Tao, N. J.; Nagahara, L. A.; Amali, I.; Tsui, R. *Phys. Rev. B* **2003**, *68*, 045302.
- Bennett, P. A.; Ashcroft, B.; He, Z.; Tromp, R. M. *J. Vac. Sci. Technol. B* **2002**, *20*, 2500–2504.